A Moisture Index for Surface Characterization over a Semiarid Area

Lesley-Ann Dupigny-Giroux and John E. Lewis

Abstract

A multispectral index, designed to describe surface moisture characteristics, was derived from the information content at the blue, near-infrared, and thermal wavelengths of Landsat Thematic Mapper imagery. The index is given by an open-ended triangle within which features of varying moisture contents are located. Although the index bears some resemblance to existing soil and vegetation indices as well as to the Tasseled Cap transformation, it differs in the way in which moisture, brightness, and vegetation information can be expressed in one locational space. The index was found to vary as a function of changes in the season, in vegetation cover, and in moisture conditions. The index was also found to be sensitive to the spatial resolution at which it was described.

Introduction

Of the many land-surface parameters that can be derived from remotely sensed inputs, surface moisture (be it of the soil or overlying vegetation canopy) is perhaps one of the least well characterized. The quantification of soil moisture presents a sufficient challenge, in that it is highly variable over space and time, and difficult to estimate directly without *in situ* measurements of thermal emissivity, surface roughness, and other key soil attributes. The problem is further compounded by varying degrees of canopy cover. Vegetation response changes at small and large spatial scales, as a result of differences in plant species, plant architecture, growth stage, and plant stress, among other factors (Jasinski and Eagleson, 1989).

The primary objective of the current study was to develop a moisture index that was sensitive to variations across a variety of surface types, and at the same time robust enough to be independent of *in situ* measurements should they be unavailable. Existing studies (Séguin *et al.*, 1991; Carlson *et al.*, 1992) have produced moisture estimates from remotely sensed inputs using coincident field measurements of soil and foliar moisture. The moisture index derived in this study does not provide actual estimates of soil moisture, but instead characterizes surface wetness relative to other features within a given scene. The use of within-scene responses allows for the comparison of moisture patterns across time. The author is currently laying the groundwork for translating the index from its current form into a calibrated mechanism whereby estimates of soil moisture could be derived.

A secondary objective was to determine whether the derived moisture index was sensitive to scale. Landsat Thematic Mapper (TM) imagery for a semiarid region in northeast Brazil was initially used to develop the index. The methodology was then applied to coarser resolution NOAA/AVHRR data, taking the differing spectral resolution of the bandwidths used by the two sensors into account.

The proposed moisture index was not developed in isolation, but resembles existing vegetation and soil indices in some respects. Its uniqueness lies in the choice of spectral information, and the complementary ways in which features can be located in multispectral (blue-infrared) space. The applicability of the entire approach, as well as its validity across different spatial resolutions, will now be presented.

Background

The moisture index differs from existing approaches that use remotely sensed inputs to parameterize vegetation or soil properties. Such techniques try to capture a high sensitivity to the property in question, with the elimination of other signals which are considered as noise.

One of the commonest ways of quantifying vegetation characteristics is the use of a vegetation index (VI), which can be defined as "a number that is generated by some combination of remote sensing bands and may have some relationship to the amount of vegetation in a given image pixel" (Ray, 1994). Such indices are primarily used to characterize greenness or biomass production. There is also the assumption of the presence of a "soil line" in spectral space (Ray, 1994). A soil line is given by the pixels that contain bare soil and dry vegetation (Jasinski and Eagleson, 1989). Vegetation indices usually involve the ratioing or linear combinations of spectral information at the red and infrared wavelengths. Band ratioing leads to the separation of vegetation data from those of soils (Ustin *et al.*, 1986), and reduces the effects of sun-sensor-target geometry variations. Among the frequently used VIs are the Simple Ratio (SR) or Ratio Vegetation Index (RVI), the Perpendicular Vegetation Index (PVI), the Greenness Vegetation Index (GVI), the Soil Adjusted Vegetation Index (SAVI), and the Greenness Above Bare Soil (GRABS). Comprehensive reviews of the computation and characteristics of these and other indices are given in Qi *et al.* (1994), Major *et al.* (1990), and Baret and Guyot (1991).

For such indices, noise is introduced by variations in soil properties (moisture content, soil color, and organic matter) and atmospheric influences. SAVI (Huete, 1988) was designed to reduce the effect of soil brightness by including a soil adjustment factor. Subsequent work on this index has produced a Modified Soil Adjusted Vegetation Index MSAVI (Qi *et al.*, 1994) in which the adjustment factor is allowed to vary depending on the soil types in the scene; TSAVI (Trans-

L. Dupigny-Giroux is with the Department of Geography, University of Vermont, Old Mill Building, Burlington, VT 05405-4170.

J.E. Lewis is with the Department of Geography, McGill University, Quebec, Canada.

Photogrammetric Engineering & Remote Sensing, Vol. 65, No. 8, August 1999, pp. 937–945.

0099-1112/99/6508–937$3.00/0

formed Soil Adjusted Vegetation Index) (Baret and Guyot, 1991), which takes the slope and intercept of the soil line into account; and the family of ARVIs (Atmospherically Resistant Vegetation Index), which introduces blue wavelengths into the NDVI to account for variations in the atmospheric aerosol content (Huete and Liu, 1994). Numerous studies (Huete and Jackson, 1988; Clevers, 1989; Baret and Guyot, 1991; Major *et al.*, 1990; Huete *et al.*, 1992; Qi *et al.*, 1994) have compared the various indices in terms of their sensitivity to soil interactions at varying vegetation cover extents. Huete and Liu (1994) have also developed MSARVI, a soil and atmospherically resistant vegetation index, to account for both soil variations and changes in the aerosol content of the atmosphere.

At the other end of the spectrum, studies on the inference of soil moisture have focused on bare soils, with the view of vegetation as a contaminant to the signal. There are three types of spectral indices of soil moisture: those employing the absolute reflectance in one or more bands; those that examine the contrast between the visible and near-infrared bands to the middle infrared; and those which contrast information at mid-infrared wavelengths only (Musick and Pelletier, 1988). It has long been established that reflectances at mid-infrared (MIR) wavelengths respond primarily to water content (Currico and Petty (1951) in Verbyla (1993)). Verbyla (1993) contends that MIR wavelengths are most useful under an extreme range of conditions, but, for less divergent situations, complications may arise as a result of changes in soil texture, soil structure, organic matter, clay and mineral composition, plant canopy, and terrain conditions. Studies which have used MIR data to infer soil moisture include Shih and Jordan (1992) who used Landsat TM7 imagery with land-use groupings within a GIS to derive qualitative surface soil moisture values. Avila *et al.* (1994) employed a ratio of the two Landsat TM-MIR bands to evaluate soil moisture. Lindsey *et al.* (1992) fused point measurements with remotely sensed ones to extrapolate estimates of soil moisture over a watershed, by using a fuzzy-c classification algorithm.

From a different approach comes the use of microwave data to quantify soil moisture values. Lakshmi *et al.* (1997) have used SSM/I-derived soil moisture with a thin-layer hydrologic model to compute cumulative monthly evaporation.

Apart from vegetation and soil indices, research has also been conducted on the quantification of plant water stress, either by using crop stress indices, or by multispectral methods involving thermal infrared (TIR) data with existing vegetation indices. Hope *et al.* (1986) used the TEGRA model to simulate surface fluxes of energy and water from vegetation, and the SAIL radiative transfer model to compute spectral VI albedo. They found a negative relationship between surface temperature and NDVI under a series of soil moisture conditions. They also suggested the division of surface temperature by the minimum canopy temperature to normalize the former for extraneous influences apart from soil moisture and canopy resistance response. Similar results were obtained by Carleton *et al.* (1994) who concluded that the low NDVI and high temperature regions for the study area in the American Midwest corresponded to cropped and moisture-stressed surface types. Crop water stress has also been quantified in terms of stress degree days in a study by Séguin *et al.* (1991), which demonstrated the usefulness of TIR data for assessing such stress conditions at a regional scale.

In all of the foregoing studies, field data have been merged with imaged data either directly or as part of a simulation, at a variety of spatial scales. Such ground truthing was not collected at the time of imaging in 1992 for the case studies to be discussed. The challenge then became to develop a method of classifying moisture across the surface, using urban areas and the Rio São Francisco (the largest river in the Brazilian northeast) as reference points. Given that stressed areas cannot be determined from TIR data without prior knowledge of their location (Rhode and Olson (1970) in Pierre *et al.* (1990)), a multispectral approach was used in conjunction with ancillary data on the vegetation and soils types present to develop the moisture index.

Study Area

The *sertão* (semiarid interior) of northeast Brazil (*nordeste*) is a delicate ecosystem characterized by periodic droughts that destroy vegetation and disrupt the agrarian economy. It is a vast area (650,000 km^2) with an extremely diverse geography, topography, and climate. A high degree of variability in the rainfall received is an inherent characteristic of this climate. Soils tend to be poor, although fertile alluvial floors can be found along the river valleys (de Andrade, 1980).

The study area is located along the middle reaches of the Rio São Francisco in the state of Bahía (Figure 1) in the southern part of the *sertão*. The most important precipitation-generating mechanisms here are the northward-moving cold fronts that induce moisture advection at the middle and upper levels of the troposphere (Kousky, pers. comm., 1992). The southerly migration of the Intertropical Convergence Zone (ITCZ) is also associated with the receipt of precipitation.

Given that drought is a cyclical component of the landscape, dryland and irrigated agricultural practices are commonplace. Cattle ranching is the most important economic activity in the *sertão*, and pastures are found along the river

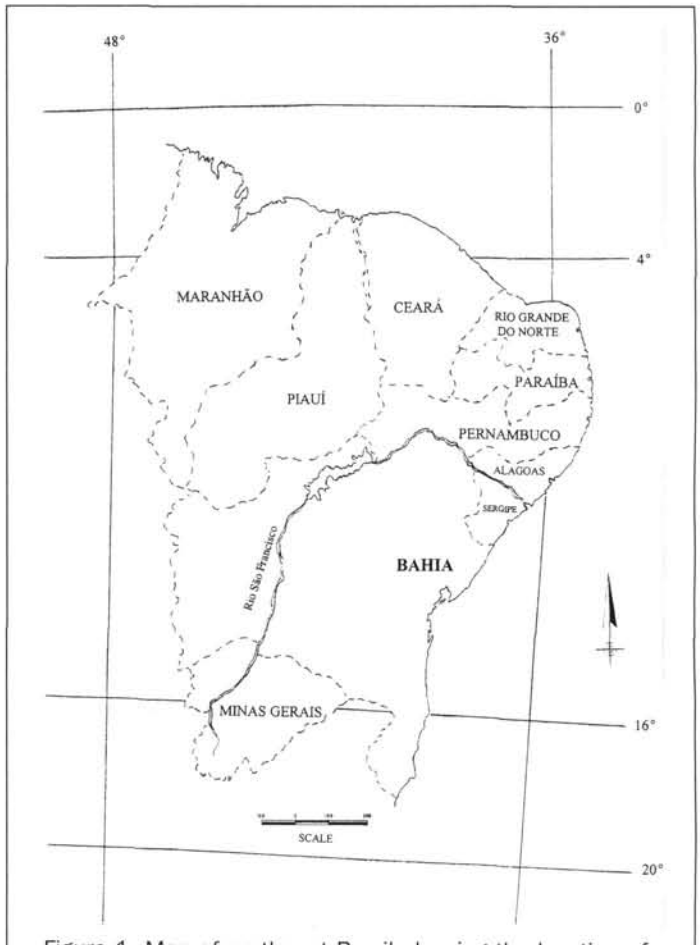

Figure 1. Map of northeast Brazil showing the location of the study area.

floodplains. Cattle and goats also graze native species like *caatinga*, which is the natural vegetation over much of the *sertão* and represents a xerophilous adaptation to the dry climate and bare soil (Webb, 1974). In appearance, the *caatinga* is a tropical scrub woodland made up of thorny, drought-resisting trees with some cacti. Many of the tree species are deciduous and remain leafless during the dry season (Webb, 1974; Magalhães and Rebouças, 1988).

Data Acquisition and Manipulation

Three Landsat-5 TM images were acquired for path 218, row 69. The time of overpass was approximately 10 30LST. The dates were chosen to reveal moisture characteristics of the surface during the different seasons. The first image was a summer acquisition from 04 January 1992, selected because of the known precipitation activity that takes place in December and January over this region of Brazil. Rainfall estimates for December 1991 and 03 January 1992 had already been computed in a previous study (Dupigny-Giroux, in preparation, 1999). With this influx of water into the system, it is likely that a greening of the vegetation would have begun. The other images were acquired during the winter of 1992 (27 May and 12 June), and were selected to provide a contrast with the January image, in terms of vegetation senescence and/or harvesting. These images were expected to show drier conditions than those in January, because the major precipitation-producing systems were located at the extreme reaches of their annual migration patterns at this time. Finally, with the winter image acquisitions being approximately two weeks apart, temporal differences in moisture level, even across the dry environment, were also expected.

Of the seven bands available on the Thematic Mapper (TM) sensor, channels 1, 3, 4, 5, and 6 were selected for each date. Bands 2 and 7 did not significantly contribute to the analysis and so were omitted. Geometric registration into a UTM (Universal Transverse Mercator) projection was performed, with resampling to a pixel size of 120 m being applied to bands 1, 3, 4, and 5, such that they matched the inherent resolution of the thermal band 6. Atmospheric scattering was accounted for using the dark-object subtraction technique as outlined in Chavez (1988). The results of this haze correction technique were checked against the crude method of determining the DN response over a water body (in this case, the Rio São Francisco) in TM5, with results in keeping with those recommended for the technique. Haze correction was essential because the indices generated under turbid atmospheric conditions yield questionable results (Huete and Jackson, 1988). From the relative scattering models used for the correction of each day, the 12 June image was the least haze affected, while the 04 January was the most. This was evident from the graininess of band 1 of the latter date. Figure 2 shows bands 1 and 3 for the 12 June image. The haze-corrected DN values for the visible and shortwave infrared bands, as well as the uncorrected thermal infrared (TIR) band, were converted to at-satellite spectral radiances (in $mWcm^{-2}\mu m^{-1}sr^{-1}$) using TIPS-ERA constants in the equation in Markham and Barker (1986; in Wilcox *et al.*, 1994). The thermal infrared band 6 spectral radiances were then converted to at-satellite temperatures (K) following Lansing and Barker (1985).

Ancillary data were provided in the form of digitized maps of the vegetation, geology, topography and soils of the area.

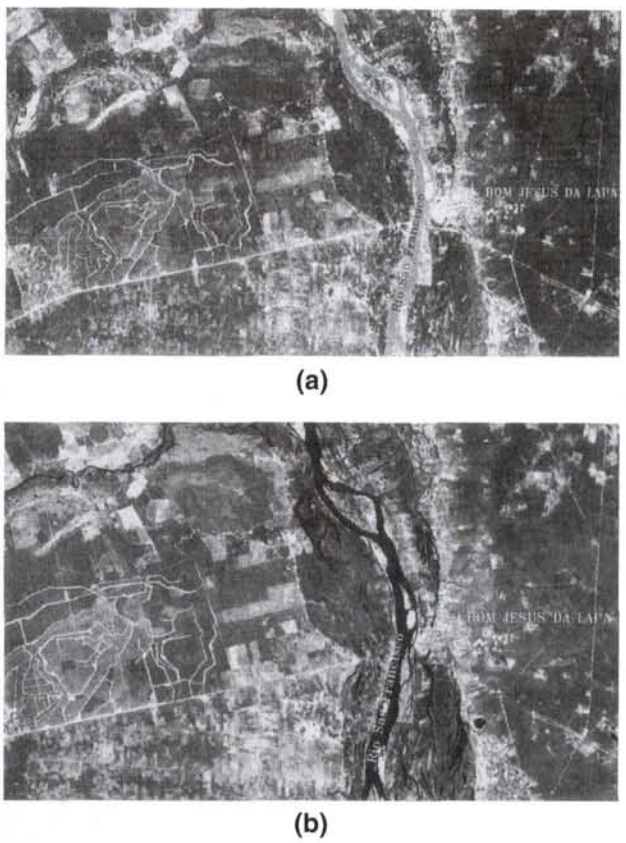

Figure 2. Extract from the full Landsat-5 TM scence (Path 218, Row 69) near the town of Bom Jesus da Lapa, Bahía for (a) channel 1 and (b) channel 5 for 12 June 1992.

Derivation of a Moisture Index

The five TM bands were initially selected for their ability to discriminate among the characteristics of various surface features. The main goal was to identify a grouping of channels that would best distinguish moisture differences across a given scene. Band 1 (at blue wavelengths) was known to provide water penetrating properties and to be able to differentiate between soil and vegetation, as well as between deciduous and evergreen species. Band 3 (at red wavelengths) provided vegetation discrimination ability, as well as a heightened contrast between vegetated and non-vegetated areas (e.g., bare soil and roads). TM4 (near-infrared (NIR)) has been widely used for its biomass determination feature, but it also allows for the separation between water bodies and vegetation. The mid-infrared (MIR) band 5 has been described as being the best band overall. Its wavelengths were sensitive to water absorption and, as such, TM5 was useful for moisture content, soil moisture, and vegetation differentiation, as well as snow versus cloud discrimination. Bands 5 and 1 were also sensitive to plant water stress. Finally, the TIR band can be used in vegetation stress analyses and soil moisture discrimination (Toselli, 1989; Lillesand and Kiefer, 1994).

Initial attempts focused on ratioing a combination of bands 3, 5, and 6. However, the resulting ratios failed to provide stable moisture descriptions for one or more of the three days under study. Similarly, poor results were obtained for the 4, 5, and 6 band grouping. One factor that may have lead to the failure of these band combinations was the nature of the vegetation present. Given the adaptation of many of the species to drought conditions, the types and/or magnitudes of changes that would be observed for broad-leaved species in a more humid environment were invalid in this context. Thus, the information content of bands 3 and 5 becomes questionable.

The moisture index that was used in the study is given

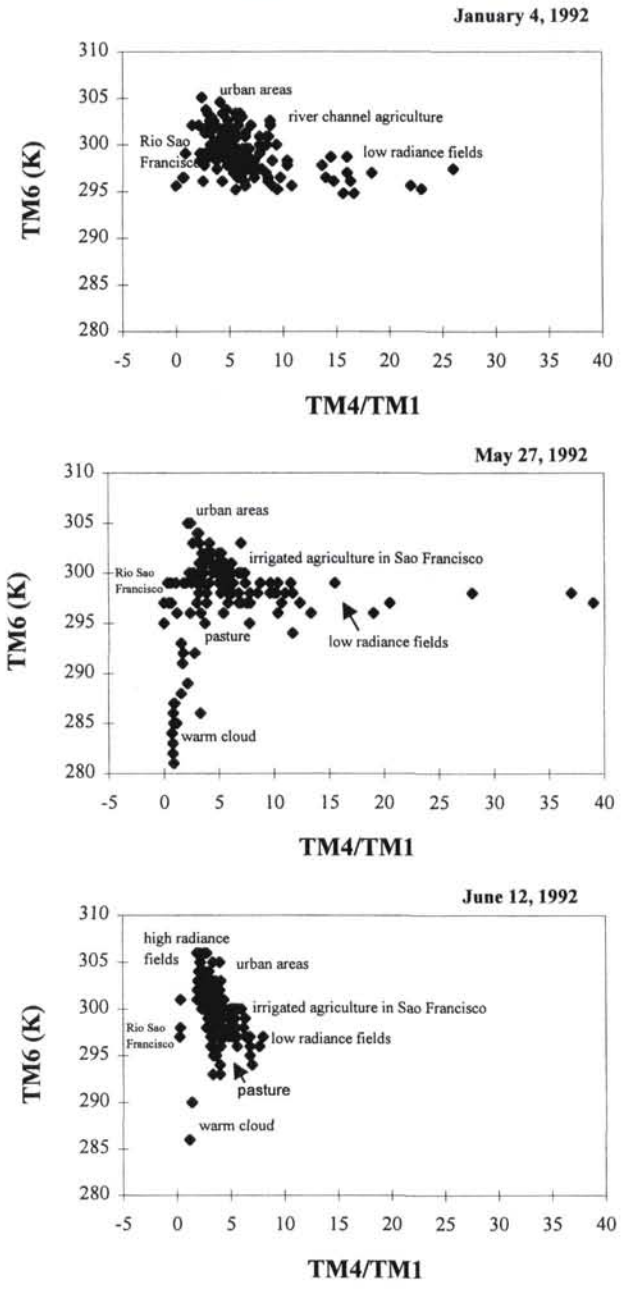

Figure 3. Scattergrams of the channel 6 temperatures vs. the NIR/blue ratio for Landsat TM data — 04 January, 27 May, and 12 June 1992.

by a scattergram of TIR temperatures against the ratio of band 4 to band 1 (TM4/1). The combination of TM1 and TM4 best captured the differences between urban areas, water bodies, and full-leaf versus leafless conditions. The TIR band was invaluable in helping to distinguish among the surface feature types that may have had similar ratio values. This was especially useful at very low ratio values where other indices like the NDVI would have grouped together very disparate feature types like rivers and roads. Figures 3a, 3b, and 3c show the corresponding scattergrams for 04 January, 27 May, and 12 June 1992. From each scattergram, three common features were observed: a vertical cutoff at ratio values of TM4/1 = 0; a second threshold at temperatures of 295K; and a line of negative slope, which completed the moisture triangle.

The TM4/1 ratios and TM6 imagery were queried for the characteristic values of the various surface types present, and these values were used in the annotation of Figure 3. Some of the more important surface features included water bodies of all types including the Rio São Francisco, pasture and agriculture along the floodplain of the foregoing river, pivot irrigation agriculture, rectangular fields of varying reflectance, irrigated agriculture in the channel of the Rio São Francisco, urban areas, roads, and cloud.

From the annotated scattergrams, it can be concluded that the vertical line TM4/1 = 0 can be described as a "water" line (see Figure 4). Cloud and water bodies fell along this line, and were differentiated by their temperatures. For example, clouds when present were always colder than 290K. The Rio São Francisco displayed a fairly constant temperature of 298K (±1K). The water line does not extend over the full range of temperatures and, as such, the triangle remains open for TM6 values greater than 298K. At the lower end, the water line can extend to temperatures of 203K or colder, found in the interiors of deep, cumulonimbi formations.

The horizontal boundary at TM6 = 295K represented completely moist conditions. It was anchored at the lower end by water bodies falling along the water line, and at the upper end by moist, fully vegetated surfaces. Surface moisture decreased and temperatures increased as one moved away from this horizontal asymptote, towards the upper apex of the moisture triangle. Thus, along an isoline parallel to this asymptote, moisture values remained constant while surface types or densities varied.

It therefore followed that the hypotenuse of the triangular relationship was essentially a moisture gradient from dry conditions at the upper apex to wet surfaces at the intersection of the slope with the TM6 = 295K line. Urban areas and fields with high radiances could be found at the upper end of the hypotenuse, where the water line does not extend, leaving the moisture triangle open. Queries of the same locations over time revealed that, as drying and/or senescence occurred, there was a movement away from the horizontal asymptote along isolines that were parallel to the hypotenuse.

Within these boundaries, the major feature types already listed could be found. Floodplain agriculture tended to gravitate towards the line TM6 = 295K, and low values of TM4/1. Fields with low reflectances tended to be somewhat warmer and exhibited higher ratio values. Urban areas, high-radiance fields and the cultivated islands in the Rio São Francisco ex-

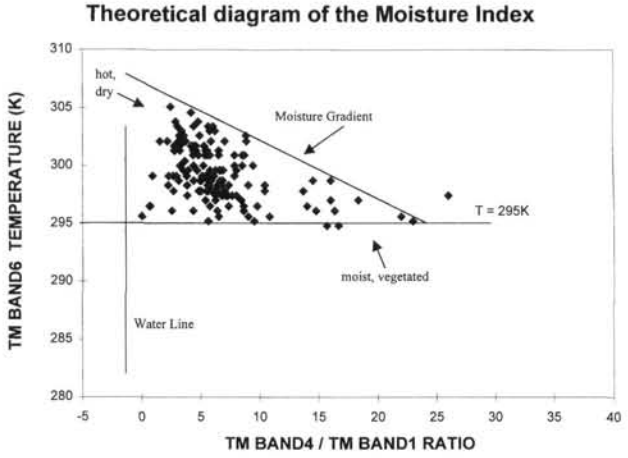

Figure 4. Theoretical diagram of the Moisture Index.

hibited similar values, but could be separated on the basis of their TM4/1 values more so than their TIR temperatures.

It has been noted that, with the exception of urban areas, the signatures of the various feature types varied with time, although their positions relative to each other in locational space was essentially unchanged. For example, the TM4/1 values for high-reflectance fields declined from the January image to the one in June. On the other hand, features like the floodplain pasture and the low-radiance fields increased in TM4/1 values from January to a maximum in May, before declining in June.

External Influences on the Moisture Index

The characteristic boundaries of the moisture triangle, as outlined above, were essentially constant from one image to the next, although the clarity with which they were defined changed with the season. The triangle was best defined for the summer (January) image, with the boundaries becoming fuzzy for the June (winter) image. One cause of this blurring could have been the decrease in vegetation cover extent that took place from January to June. As Figure 5a shows, the NIR/Red scattergram for January indicates an almost complete canopy cover. By contrast, the NIR/Red scatter for June (Figure 5b) revealed incomplete canopy coverage and the possible presence of shadows (Jasinski and Eagleson, 1989).

A second factor which affected the shape of the moisture triangle was the nature of the existing and antecedent moisture conditions. The 04 January image was known to have been preceded by a day of precipitation inputs on 03 January. The range of observed TM4/1 ratio values was large, and the leftmost part of the moisture triangle was close to the water line of TM4/1 = 0. The June image was much drier overall, such that, not only was the TM4/1 ratio range substantially smaller but, in addition, the vertical boundary had shifted away from the water line in the direction of decreasing moisture. Attempts to establish a relationship between antecedent rainfall and the TM4/1 values or TM6 temperatures of the following day yielded poor results.

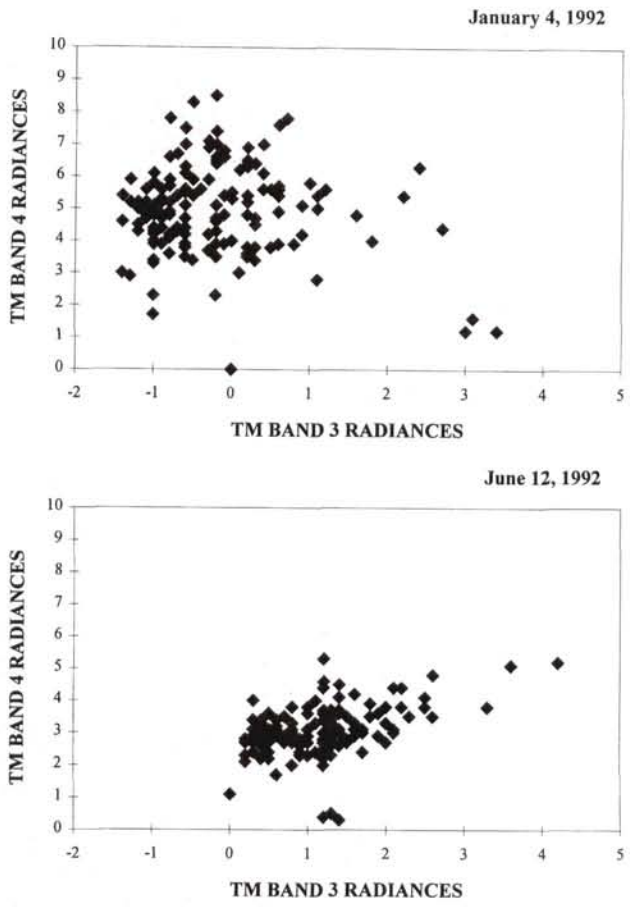

Figure 5. Scattergrams of the near-infrared vs. red radiances for Landsat TM data — 04 January and 12 June 1992.

Effect of Scale on the Moisture Index

A secondary objective of the current research was to ascertain whether the effectiveness/results of the moisture index triangle were maintained in scaling up from the original 120-m pixel size to coarser spatial resolutions. To this end, 1-km resolution NOAA/AVHRR images that coincided with the TM dates were selected. The available bands from the AVHRR imagery did not coincide exactly with those of the Thematic Mapper in terms of their acquisition times (a lag of 4 hours), their bandwidths, and their sensitivity in certain regions of the electromagnetic spectrum. The NOAA/AVHRR satellite has two sensors in the TIR bandwidth that are covered by only one sensor on the Landsat satellite, but lacks a sensor at the blue wavelengths which correspond to TM1.

In order to overcome the incompatibility of bands between the two satellites, the moisture index triangle was modified to be defined in the TM6-TM4/3 locational space for the TM sensor. This grouping of bands exhibited a similar information content as TM6-TM4/1, but was not selected over the latter because of its instability for the January image. The corresponding AVHRR locational space was given by T4-A2/1, where T4 was the at-sensor temperature (K) of Channel 4, with A1 and A2 being the spectral radiances for Channels 1 and 2, respectively. The ratioed image and T4 band were then queried using the same points as for the TM data, with the resulting scattergrams for the AVHRR imagery being given on Figure 6.

At a first glance, the AVHRR scattergrams (with the exception of the 12 June diagram) did not seem to resemble their TM counterparts. For 04 January and 27 May, the triangular shape of the points in space appeared to have been compressed over the range of temperatures. This was misleading, however, because the triangular portion of the scattergram was constrained over the same range (295 to 310K) as had been the case for the TM diagrams. The apparent compression of the thermal range was due to the presence of significant cloud coverage which had been absent earlier in the day when the TM images were acquired. The clouds present on the scattergram were warm in nature (>245K), and occupied the thermal range of 270 to 290K. Thus, in terms of their temperatures, the clouds occupied the same portion of locational space as they did on the TM diagrams. It should be noted that the clouds present on the AVHRR image were colder and deeper than had been the case for the earlier TM scenes. However, due the nature of the querying process, these cold clouds were not captured. One final caveat is that the A2/1 values for the clouds were not zero as it had been for the TM ratio, and this, coupled with similar non-zero values for the other water bodies present, implies the absence of a water line for the January and May AVHRR imagery.

The T4-A2/1 scattergram for 12 June resembled the triangular nature of the TM index with some differences. Like the other AVHRR scattergrams, there was no water line which acted as an asymptote at low ratio values. This was related to the fact that the lower boundary of T4 = 295K did not extend over the entire A2/1 range, which, when coupled with the lack of a water line, led to the absence of a perpendicular vertex at T4 = 295K, A2/1 = 0. It should be remembered

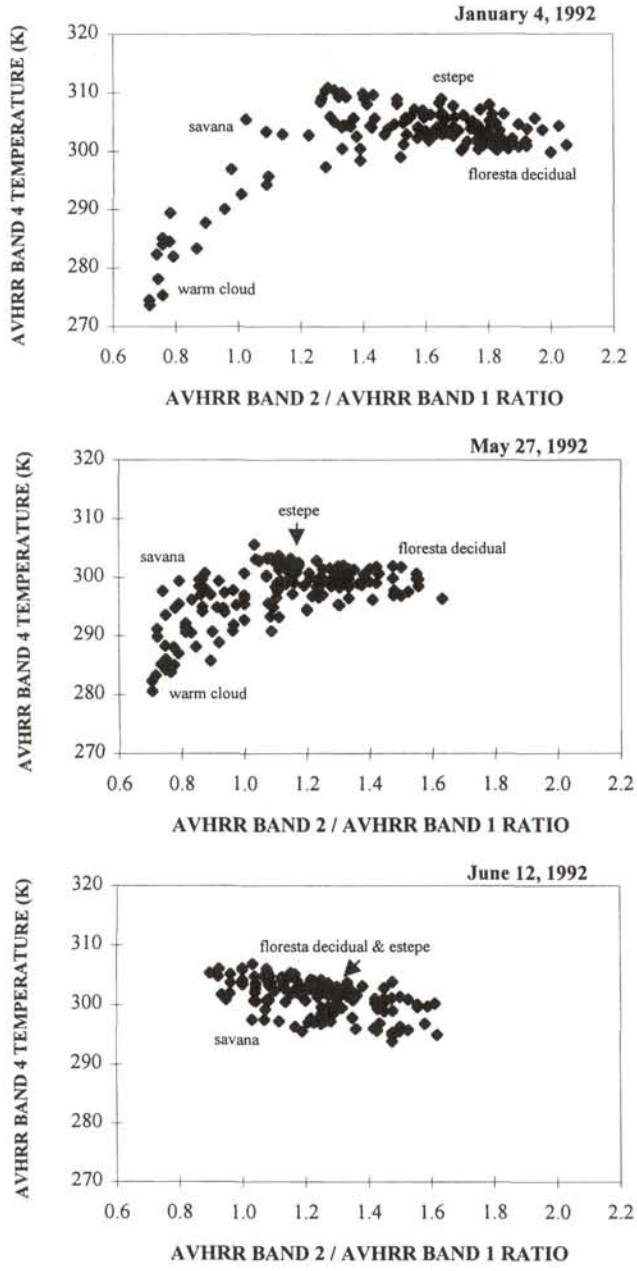

Figure 6. Scattergrams of the channel 4 temperatures vs. near-infrared/red ratio for NOAA/AVHRR data — 04 January, 27 May, and 12 June 1992.

that features, such as water bodies and floodplain agriculture, tended to gravitate towards this vertex in the corresponding TM triangles. It can therefore be concluded that the 12 June image was drier than the others, and cloud free as well. The asymptotic values for the 12 June scene was at about A2/1 = 0.85, instead of at A2/1 = 0.7, as it was for January and May.

From the foregoing, it can be observed that the moisture index did present some similarities at the two resolutions. The characteristic triangular shape was preserved, even though it was not as well-defined as was observed for the TM diagrams. Differences across resolution included the nature of the vertical asymptote, as well as the much reduced range of values for A2/1 compared to either TM4/1 or TM4/3. It becomes imperative to examine these differences in order to account for the divergence in results between the TM and AVHRR imagery.

Differences in Mechanisms Across Scale

There are four main reasons that may account for the lack of similarity between the moisture index triangles of the Landsat and NOAA/AVHRR satellites. The first and perhaps most evident is related to the spatial resolution of each sensor. The most commonly used measure of this is the instantaneous field-of-view (IFOV), which, in the case of the TM sensor, is 30 m for the visible (1, 3) and shortwave infrared (4, 5) bands, but 120 m for the thermal infrared band. The IFOV of the NOAA/AVHRR sensor is approximately 1.1 km at nadir. Even though the TM bands 1, 3, 4, and 5 were resampled to 120 m to match the resolution of the TIR band, the difference in the spatial resolving powers of the two satellites (120 m versus 1.1 km) is clearly evident in the land surface types that could be detected. For example, the TM sensors were able to detect the various characteristics of the Rio São Francisco channel, including the cultivated islands, while the same river was not observable on the coarser scale NOAA/AVHRR imagery. Similarly, the variations in spectral radiance within fields and between fields observed at the finer TM resolution were lost as pixel size increased. At the 1.1-km resolution, only broad patterns in the vegetation types could be observed, e.g., open scrub (*caatinga*) versus grassland-forest ecotone (*contato-estepe-floresta estacional ecotono*). Finally, urban areas were also below the resolution of the AVHRR sensor. It was this feature type as well as the high-radiance fields that helped to define the upper vertex of the TM version of the moisture index at the high thermal values and low ratio ones. For the coarser AVHRR index, the non-resolution of settlement patterns and individual fields meant that key data needed to define the uppermost apex of the resulting triangle were absent.

A second contributing factor was the difference in spectral resolution between the satellites. The spectral resolution refers to the width of the spectral bands over which information is collected. For the red wavelengths, there was some overlap between the AVHRR (0.58 μm) and TM (0.63 to 0.69 μm) sensors. The bandwidth of the AVHRR NIR wavelengths (0.72 to 1.1 μm) actually encompasses that of the TM NIR radiometer (0.76 to 0.9 μm). A wider bandwidth tends to average out differences in the surface being imaged (Mather, 1989) and, therefore, the overall level of differentiability in the TIR-NIR/Red space was lower for the AVHRR sensor than for the TM sensor. Measurements from these wider bandwidths tend to be more susceptible to atmospheric attenuation (Goward *et al.*, 1991). Finally, the use of AVHRR Channel 4 (10.3 to 11.3 μm), which only covers about one-half of the width of TM band 6 (10.5 to 12.5 μm), implies that the information content at the upper TIR wavelengths was not included in the AVHRR-based triangle.

Apart from the platform characteristics, one other cause of the non-congruity between the two satellites was the effect of seasonality. This was clearly evident, not only in the vegetation cover differences between the summer and winter images, but also in the thermal range. It should be noted that, for the finer-scale TM images, the temperature ranges across the seasons were fairly constant whereas, for the AVHRR scenes, the range was larger for the summer imagery. This may be partly due to the presence of precipitation-producing clouds that extended the range into colder temperatures.

Finally, the time lags between the morning TM images and the afternoon AVHRR scenes contributed to the differences in synoptic conditions, thermal variations, and moisture changes across the diurnal period.

Discussion

The moisture index described herein differs from vegetation indices or soil moisture indices. Unlike vegetation indices, which should ideally be highly sensitive to vegetation, to the exclusion of the soil background, with a small influence from the atmospheric path radiance (Tueller, 1987), the present approach utilizes the response of various surface types present in a given scene. Similarly, the index is not constrained to bare soil surfaces only. The ability to locate features along moisture gradient lines should provide a useful tool in determining the effectiveness with which precipitation inputs cascade through the system.

Like the Normalized Difference Vegetation Index (NDVI), bare soil and water have ratio values close to zero. However, the choice of bands used in the current index allowed for the differentiation between these two feature types which are vastly different in terms of their moisture and thermal characteristics. Water bodies of all types, including supercooled water (i.e., clouds), were clustered together along a "water" line. The water line acted as a vertical asymptote, such that the drier the scene, the more the entire locational space shifted towards higher ratio values and away from the water line. This shift away from the water line also occurred in going from fine to coarser resolutions. A corollary to this rightward shift with decreasing moisture or increasing scale was the fact that it also resulted in a decreased range of TM4/1. In spite of this, similar thermal ranges (280 to 310K for the TM and 270 to 310K for the AVHRR) were observed at both resolutions.

The moisture index triangle bears a striking resemblance to the Tasseled Cap transformation of Kauth and Thomas (1976), who originally derived it for Landsat MSS (Multispectral Scanner) data. For MSS data, the transformation represents a planar distribution of the data due to a correlation of plant and soil properties between the two visible and two infrared bands present on this sensor. There are two axes of variability — brightness and greenness. In applying the transformation to six non-thermal bands on the TM sensor, Crist and Cicone (1984) discovered an additional wetness dimension that was initially thought to be a sole function of soil moisture status. The brightness and wetness dimensions together define the Plane of Soils, which contains only soil data. Changes in brightness are correlated to relative changes in soil moisture content, but an exact association between brightness values and a given soil moisture content value could not be estimated. The Plane of Vegetation for fully vegetated data is given by the greenness and brightness where the latter is used to characterize soil moisture status. Partially vegetated regions fell into a Transition Zone defined by the wetness and greenness dimensions (Crist and Cicone, 1985).

The current moisture index is more triangular in shape than the cone-shaped features given by the Plane of Soils or the Plane of Vegetation. The horizontal boundary (T = 295K) may be similar to the greenness dimension in the Transition Zone, while the vertical asymptote may represent a combination of wetness and brightness information as one moves from a dark water body to bright urban surfaces. This difference in the interpretation of the vertical line reflects the use of thermal infrared data to define the locational space, a band that is not used in the Tasseled Cap transformations.

In a study by Tucker and Choudhury (1987), using the NIMBUS-7 SSMR 37GHz brightness temperatures and NOAA/AVHRR NDVI values, graphical results that were very similar to those of the moisture index derived in the current study were observed. Working over cropped areas in the American Midwest, Carleton *et al.* (1994) also discovered a negative relationship between the NDVI and surface temperature, such that low NDVI values were associated with high temperatures (on the order of 301 to 306K).

Following from the fact that the vertical line extends from a water body surface (which is essentially wet) to urban areas which, in the absence of rainfall to wet the surface, are essentially dry, one way of providing a qualitative estimate of moisture would be to find the intersection of the water-urban areas line with those parallel to the hypotenuse. A sliding scale of moisture (e.g., 1 for the water body and 0 for the urban areas) could be defined, such that the intersection of the isomoisture lines with the water-urban line would yield a relative value of moisture. Field measurements could then be used to translate this relative sliding scale into actual moisture content values. This approach is similar in concept to the moisture availability studies of Carlson (1986).

Summary and Conclusions

A multispectral index has been proposed for use in describing surface moisture characteristics. The choice of the blue, near-infrared, and thermal bands produced a characteristic triangular shape, with features containing water in any state forming a vertical asymptote. Fully vegetated areas formed a second horizontal asymptote, with the triangle being completed by an isomoisture line.

While bearing some resemblance to existing vegetation and soil indices, as well as to the Tasseled Cap transformation, the current index differs in its combination of information on moisture, brightness, and vegetation into one feature space. Brightness increases as one moves up the water line, and moisture increases along a line perpendicular to the hypotenuse of the triangle.

The moisture index was found to vary as a function of season, due to changes in the vegetation cover. The index was also sensitive to existing and antecedent moisture conditions.

In applying the index to coarser resolution imagery, the characteristic triangular shape was preserved, although the thermal range appeared to have been compressed due to an increased contribution from cloud. Due to factors such as differences in spectral and spatial resolution, certain features were not imaged by the AVHRR sensor, and this led to the omission of certain parts of the triangle. The range of the ratio values appeared to decrease with coarser resolutions.

In its present form, the proposed index is somewhat theoretical, the results of which could be refined and enhanced in three ways. The first major area would involve conducting a field experiment in which coincident measurements of surface moisture (both foliar and soil) were made, along with radiometric readings in the blue, NIR, and TIR wavelengths. The entire experiment should be set up to coincide with the local transit time of the satellite from which the index would be later derived. The relationship between the moisture distributions and properties at the ground level could then be scaled up to the resolution of the satellite, and thus provide a calibration for the moisture index values.

A corollary of the above field experiment would be the exploration of the influences of such factors as canopy properties, atmospheric conditions, and soil variations (apart from changes in water content) on the characteristics of the moisture index triangle. Special attention should be paid to the dominant vegetation types present, such as *caatinga* and pasture, as well as the non-subsistence crops like cotton.

Finally, given that 1992 was a drought year, the validity of the index should be tested by applying it to a non-drought year. It should also be applied across all the seasons of both drought and non-drought time frames, for the assessment of changes and/or similarities.

Acknowledgments

The authors wish to thank Mr. Lawrence A. Houston for his invaluable contributions in the data manipulation involved

in this study, as well as the Instituto Nacional de Pesquisas Espaciais for their asistance in the acquisiion of the Landsat imagery.

References

Avila, V.E., M. Yoshida, M.A.M. Evangelista, and J.D. Rondal, 1994. A methodology for soil moisture condition detection using remotely sensed data, *Asian-Pacific Remote Sensing Journal*, 7(1): 109–118.

Baret, R., and G. Guyot, 1991. Potentials and limits of vegetation indices for LAI and APAR assessment, *Remote Sensing of Environment*, 35:161–173.

Carleton, A.M., D. Travis, D. Arnold, R. Brinegar, D.E. Jelinski, and D.R. Easterling, 1994. Climate-scale vegetation-cloud interactions during drought using satellite data, *International Journal of Climatology*, 14:593–623.

Carlson, T.N., 1986. Regional-scale estimates of surface moisture availability and thermal inertia using remote thermal measurements, *Remote Sensing Reviews*, 1:197–247.

Carlson, T.N., E.M. Perry, and T.J. Schmugge, 1990. Remote estimation of soil moisture availability and fractional vegetation cover for agricultural fields, *Agricultural and Forest Meteorology*, 52(1–2):45–69.

Carter, G.A., 1994. Ratios of leaf reflectances in narrow wavebands as indicators of plant stress, *International Journal of Remote Sensing*, 15(3):697–703.

Chavez, Jr., P.S., 1988. An improved dark-object subtraction technique for atmospheric scattering correction of multispectral data, *Remote Sensing of Environment*, 24:459–479.

Clevers, J.G.P.W., 1989. The application of a weighted infrared-red vegetation index for estimating leaf area index by correcting for soil moisture, *Remote Sensing of Environment*, 29:25–37.

Coll, C., V. Caselles, J.A. Sobrino, and E. Valor, 1994. On the atmospheric dependence of the split-window equation for land surface temperature, *International Journal of Remote Sensing*, 15(1): 105–122.

Crist, E.P., and R.C. Cicone, 1984. A physically-based transformation of Thematic Mapper Data — The TM Tasseled Cap, *IEEE Transactions on Geoscience and Remote Sensing*, GE-22(3):256–263.

———, 1985. Thematic Mapper spectral dimensionality and data structure, *Landsat-4 Science Characterization Early Results, Volume III-Thematic Mapper, Part 2* (J.L. Barker, editor), NASA.

de Andrade, M.C., 1980. *The Land and People of Northeast Brazil*, University of New Mexico Press, Albuquerque.

França, G.B., and A.P. Cracknell, 1994. Retrieval of land and sea surface temperature using NOAA-11 AVHRR data in north-eastern Brazil, *International Journal of Remote Sensing*, 15(8):1695–1712.

Gilford, M.T., M.J. Vojtesak, G. Myles, R.C. Bonam, and D.L. Martens, 1992. *South America South of the Amazon River - A Climatological Study*, USAF Environmental Technical Applications Center, Scott Air Force Base, Illinois.

Goward, S.N., B. Markham, D.G. Dye, W. Dulaney, and J. Yang, 1991. Normalized difference vegetation index measurements from the Advanced Very High Resolution Radiometer, *Remote Sensing of Environment*, 35:257–277.

Hope, A.S., D.E. Petzold, S.N. Goward, and R.M. Ragan, 1986. Simulated relationships between spectral reflectance, thermal emissions, and evapotranspiration of a soyabean canopy, *Water Resources Bulletin*, 22(6):1011–1019.

Huete, A.R., 1988. A soil-adjusted vegetation index (SAVI), *Remote Sensing of Environment*, 25:295–309.

Huete, A.R., and R.D. Jackson, 1988. Soil and atmosphere influences on the spectra of partial canopies, *Remote Sensing of Environment*, 25:89–105.

Huete, A.R., and C.J. Tucker, 1991. Investigation of soil influences in AVHRR red and near-infrared vegetation index imagery, *International Journal of Remote Sensing*, 12(6):1223–1242.

Huete, A.R., G. Hua, J. Qi, A. Chehbouni, and W.J.D. van Leeuwen, 1992. Normalization of multidirectional red and NIR reflectances with the SAVI, *Remote Sensing of Environment*, 41:143–154.

Huete, A.R., and H.Q. Liu, 1994. An error and sensitivity analysis for the atmospheric- and soil-correcting variants of the NDVI for the MODIS-EOS, *IEEE Transactions on Geoscience and Remote Sensing*, 32(4)897–905.

Jasinski, M.F., and P.S. Eagleson, 1989. The structure of red-infrared scattergrams of semivegetated landscapes, *IEEE Transactions on Geoscience and Remote Sensing*, 27(4):441–451.

Kauth, R.J., and G.S. Thomas, 1976. The tasseled-cap — A graphic description of the spectral-temporal development of agricultural crops as seen by Landsat, *Proceedings of Symposium on Machine Processing of Remotely Sensed Data*, Purdue University, West Lafayette, Indiana, pp. 41–51.

Lakshmi, V., E.F. Wood, and B.J. Choudhury, 1997. Evaluation of special sensor microwave/imager satellite data for regional soil moisture estimation over the Red River Basin, *Journal of Applied Meteorology*, 36(10):1309–1328.

Lansing, J.C., and J.L. Barker, 1985. Thermal band characterization of the Landsat-4 Thematic Mapper, *Landsat-4 Science Characterization Early Results, Volume III-Thematic Mapper, Part 2* (J.L. Barker, editor), NASA.

Leprun, J.-C., and M. Molinier, 1995. Drought and its consequences on the Nordeste region of Brasil, *Sécheresse*, 1(6):23–33.

Lillesand, T.M., and R.W. Kiefer, 1994. *Remote Sensing and Image Interpretation*, Third Edition, John Wiley & Sons, New York.

Lindsey, S.D., R.W. Gunderson, and J.P. Riley, 1992. Spatial distribution of point soil estimates using Landsat TM data and fuzzy-c classification, *Water Resources Bulletin*, 28(5):865–875.

Magalhães, A.R., and O.E. Rebouças, 1988. Introduction: Drought as a policy and planning issue in Northeast Brazil, *The Impacts of Climate Variations on Agriculture, Vol. 2, Assessments in Semi-Arid Regions* (M.L. Parry, T.R. Carter, and N.T. Konijn, editors), Kluwer Academic Publishers.

Major, D.J., F. Baret, and G. Guyot, 1990. A ratio vegetation index adjusted for soil brightness, *International Journal of Remote Sensing*, 11(5):727–740.

Mather, P.M., 1989. *Computer Processing of Remotely-Sensed Images*, John Wiley & Sons, Toronto.

Matthews, K.B., A. Macdonald, R.J. Aspinall, G. Hudson, A.N.R. Law, and E. Paterson, 1994. Climatic soil moisture deficit — Climate and soil data integration in a GIS, *Climate Change*, 28:273–287.

Musick, H.B., and R.E. Pelletier, 1988. Response to soil moisture of spectral indexes derived from bidirectional reflectance in Thematic Mapper wavebands, *Remote Sensing of Environment*, 25: 167–184.

Pierre, L.L., S.W. Running, and G.A. Riggs, 1990. Remote detection of canopy water stress in coniferous forests using the NS001 Thematic Mapper Simulator and the Thermal Infrared Multispectral Scanner, *Photogrammetric Engineering & Remote Sensing*, 56(5):579–586.

Ponce, V.M., 1995. Management of droughts and floods in the semiarid Brazilian Northeast — The case for conservation, *Journal of Soil and Water Conservation*, 50(5):422–431.

Qi, J., A. Chebouni, A.R. Huete, Y.H. Kerr, and S. Sorooshian, 1994. A modified soil adjusted vegetation index, *Remote Sensing of Environment*, 48:119–126.

Ray, R., 1994. A FAQ on vegetation in remote sensing (ftp from **kepler.gps.caltech.edu**).

Reutter, H., F.-S. Olesen, and H. Fischer, 1994. Distribution of the brightness temperature of land surfaces determined from AVHRR data, *International Journal of Remote Sensing*, 15(1):95–104.

Running, S.W., 1990. Estimating terrestrial primary productivity by combining remote sensing and ecosystem simulation, *Remote Sensing of Biosphere Functioning* (R.J. Hobbs and H.A. Mooney, editors), Springer-Verlag, New York.

Séguin, B., J.-P. Lagouarde, and M. Savane, 1991. The assessment of regional crop water conditions from meteorological satellite thermal infrared data, *Remote Sensing of Environment*, 35:141–148.

Shih, S.F., and D.D. Jordan, 1992. Landsat mid-infrared data and GIS in regional surface soil-moisture assessment, *Water Resources Bulletin*, 28(4):713–719.

———, 1993. Reply to Discussion of "Landsat Mid-Infrared Data and

GIS in Regional Surface Soil-Moisture Assessment," by David L. Verbyla, *Water Resources Bulletin*, 29(2):313–315.

Toselli, F., 1989. Applications of remote sensing to agrometeorology, *Proceedings of a Course held at the Joint Research Centre of the Commission of the European Communities in the Framework of the Ispra-Courses*, Ispra, Varese, Italy, 6–10 April 1987, Kluwer Academic Publishers, Boston.

Tucker, C.J., and B.J. Choudhury, 1987. Satellite remote sensing of drought conditions, *Remote Sensing of Environment*, 23:243–251.

Tueller, P.T., 1987. Remote sensing science applications in arid environments, *Remote Sensing of Environment*, 23:143–154.

Verbyla, D.L., 1993. Discussion of "Landsat Mid-Infrared Data and GIS in Regional Surface Soil-Moisture Assessment," by Sun F. Shih and Jonathan D. Jordan, *Water Resources Bulletin*, 29(2)309–311.

Webb, K.E., 1974. *The Changing Face of Northeast Brazil*, Columbia University Press, New York.

Wilcox, C. Hill, B.E. Frazier, and S.T. Ball, 1994. Relationship between soil organic carbon and Landsat TM data in eastern Washington, *Photogrammetric Engineering & Remote Sensing*, 60(6):777–781.

(Received 09 July 1997; revised and accepted 09 September 1998)